

THE UCSD RADIO-SELECTED QUASAR SURVEY FOR DAMPED Ly α SYSTEMS

REGINA A. JORGENSEN¹, ARTHUR M. WOLFE¹, JASON X. PROCHASKA², LIMIN LU³, J. CHRISTOPHER HOWK⁴, JEFF COOKE^{1,5}, ERIC GAWISER⁶, & DAWN M. GELINO⁷

Accepted to ApJ: August 11, 2005

ABSTRACT

As large optical quasar surveys for DLAs become a reality and the study of star forming gas in the early Universe achieves statistical robustness, it is now vital to identify and quantify the sources of systematic error. Because the nature of optically-selected quasar surveys makes them vulnerable to dust obscuration, we have undertaken a radio-selected quasar survey for DLAs to address this bias. We present the definition and results of this survey. We then combine our sample with the CORALS dataset to investigate the H I column density distribution function $f_{\text{HI}}(N, X)$ of DLAs toward radio-selected quasars. We find that $f_{\text{HI}}(N, X)$ is well fit by a power-law $f_{\text{HI}}(N, X) = k_1 N^{\alpha_1}$, with $\log k_1 = 22.90$ and $\alpha_1 = -2.18^{+0.20}_{-0.26}$. This power-law is in excellent agreement with that of optically-selected samples at low N_{HI} , an important yet expected result given that obscuration should have negligible effect at these gas columns. However, because of the relatively small size of the radio-selected sample, 26 DLAs in 119 quasars, $f_{\text{HI}}(N, X)$ is not well constrained at large N_{HI} and the first moment of the H I distribution function, Ω_g , is, strictly speaking, a lower limit. The power-law is steep enough, however, that extrapolating it to higher column densities implies only a modest, logarithmic increase in Ω_g . The radio-selected value of $\Omega_g = 1.15^{+0.37}_{-0.38} \times 10^{-3}$, agrees well with the results of optically-selected surveys. While our results indicate that dust obscuration is likely not a major issue for surveys of DLAs we estimate that a radio-selected sample of ≈ 100 DLAs will be required to obtain the precision necessary to absolutely confirm an absence of dust bias.

Subject headings: Galaxies: Evolution, Galaxies: Intergalactic Medium, Galaxies: Quasars: Absorption Lines

1. INTRODUCTION

The introduction of large data sets from surveys such as the Sloan Digital Sky Survey (SDSS) has made possible statistically significant studies of Damped Ly α systems (DLAs) (Prochaska, Herbert-Fort, & Wolfe 2005, hereafter PHW05), quasar absorption systems defined as having an H I column density $N_{\text{HI}} \geq 2 \times 10^{20} \text{ cm}^{-2}$ and which contain most of the neutral gas in the redshift interval $z=[0, 5]$ (Wolfe, Gawiser, & Prochaska 2005). These large surveys for DLAs shed light on the history of the neutral gas content of the Universe and show how it is affected by star formation and gas replenishment. However, one major problem consistently affects magnitude-limited optical surveys: the issue of intervening dust and the possibility of obscuration bias. Because the metallicities of DLAs can be as high as 1/3 solar and are always above 1/1000 solar (Prochaska 2003), the presence of dust in these objects is not surprising. Specifically, evidence from element abundance patterns suggests the presence of depletion (Pettini

et al. 1999), while evidence for differential reddening suggests that dust obscuration is possible (Pei & Fall 1995). Dust obscuration in optically-selected surveys could be introducing a selection bias against DLAs whose high dust optical depth would hide the background quasar. This effect could seriously impact the results of statistics and derived values like Ω_g , the cosmological density of neutral gas (see Pei & Fall (1995)), particularly since high column density systems that dominate Ω_g , would be theoretically most likely to have strong dust obscuration. Here and throughout the paper we will use Ω_g to mean Ω_g^{DLA} , the neutral gas contained in systems defined as being DLAs, i.e. with an H I surface density $N_{\text{HI}} \geq 2 \times 10^{20} \text{ cm}^{-2}$. For a detailed discussion of the rationale behind this choice, see PHW05.

Because radio observations are insensitive to the presence of dust, a radio-selected sample of quasars does not suffer from this dust obscuration selection effect. Therefore, a radio-selected survey is a check on the possible introduction of biases in the magnitude-limited, optical surveys. One previous survey, the Complete Optical and Radio Absorption Line System (CORALS) survey by Ellison et al. (2001), attempted to answer the question of the importance of dust obscuration by selecting quasars from the Parkes quarter-Jansky Flat-spectrum Radio Survey (Jackson et al. 2002), and then following up with optical observations of the selected quasars, regardless of magnitude, to search for the presence of DLAs. Ellison et al. found a slightly higher incidence of DLAs than that found by optical surveys. From their measurement of Ω_g , Ellison et al. concluded that the effects of dust could be suppressing the magnitude-limited value of Ω_g by no more than a factor of two.

The radio-selected surveys were motivated by several

¹Department of Physics, and Center for Astrophysics and Space Sciences, University of California, San Diego, Gilman Dr., La Jolla; CA 92093-0424; regina@physics.ucsd.edu, awolfe@ucsd.edu

²Department of Astronomy and Astrophysics, UCO/Lick Observatory; University of California, 1156 High Street, Santa Cruz, CA 95064; xavier@ucolick.org

³Lucent Technologies, Naperville, IL.

⁴Dept. of Physics, University of Notre Dame, Notre Dame, IN 46556

⁵Center for Cosmology, University of California, Irvine, Irvine CA 92697-4575; cooke@uci.edu

⁶NSF Astronomy & Astrophysics Postdoctoral Fellow, Yale Astronomy Department and Yale Center for Astronomy & Astrophysics, PO Box 208101, New Haven, CT 06520-8101

⁷Michelson Science Center, Caltech, MS 100-22, 770 South Wilson Avenue, Pasadena, CA 91125

studies which indicated that dust obscuration would significantly bias the results of Ω_g and other quantities derived from optical surveys. Fall & Pei (1993) constructed models to predict the possibility of dust obscuration of quasars and found that between 10 and 70% of quasars at $z = 3$ could be obscured, resulting in an underestimate of Ω_g by the optical surveys. Recently, Wild & Hewett (2005) report on a survey of SDSS quasars for Ca II absorption-line systems with $0.84 < z_{abs} < 1.3$. Using Ca II along with Fe and Mg lines, they claim that most of their sample likely contains DLAs and a significant amount of reddening. By modeling the reddening of these systems they make an estimate that they are missing $\approx 40\%$ of Ca II systems from the SDSS due to dust obscuration, which they compare favorably to the upper limit of the CORALS survey.

On the other hand, the SDSS-DR3 survey which found 525 DLAs (PHW05), indicates that a dust bias, if present, is not an important effect. Prochaska et al. examine their results as a function of quasar magnitude, separating out the brightest 33% and the faintest 33% of the sample in each of four redshift bins. While there is not a statistically significant difference in the line density, they measure 40% higher Ω_g values towards brighter quasars at the 95% c.l. Since this is the opposite effect of what the dust bias would naively imply (a dust bias may imply that $\Omega_g^{bright} < \Omega_g^{faint}$, since the brightest observed quasars should have less foreground dust obscuration which implies a smaller N_{HI} value and hence smaller Ω_g), the SDSS-DR3 results with a statistically significant higher value of Ω_g towards brighter quasars point to the conclusion that dust obscuration is not an important effect. When Murphy & Liske (2004) examined the results of the SDSS-DR2, a sample including 70 DLAs they found no evidence for reddening. After examining the much larger SDSS-DR3 Murphy et al. (2005) find evidence for reddening, but at a very low level – the implied dust to gas ratio is less than 0.02, where dust to gas ratio is defined relative to that of the Milky Way (see equation 7 of Wolfe et al. (2003)). However, with all of these studies it is important to remember that optical samples cannot measure dust bias in objects so heavily extincted that they are missing from the samples. As larger optical surveys for DLAs become feasible, due to surveys like the SDSS, and the statistical uncertainties become $< 5\%$, potential causes of systematic uncertainties, such as dust obscuration, must be fully understood.

In this paper we will present the results of a radio-selected quasar survey that was undertaken by our group. This UCSD sample is approximately the same size as the CORALS sample and presents a comparable assessment of dust obscuration. We will analyze the combined results, attempt to assess the H I column density distribution function, $f_{HI}(N, X)$, and show that our results for Ω_g do not differ in a statistically significant way from the results of optically-selected surveys, therefore suggesting that dust obscuration is most likely not a major problem affecting optically-selected quasar samples for DLAs.

The organization of this paper is as follows: In § 2 we describe the UCSD quasar sample, DLA identification method and analysis processes. In § 3 we review the standard DLA statistical analysis methods. We discuss the results of the UCSD, CORALS and combined samples in

§ 4, as well our process for dealing with the Empty Fields. And finally, in § 5 we will compare our results with the most recent optical surveys.

Throughout the paper we will use the following cosmological parameters (Bennett et al. 2003): $\Omega_\Lambda = 0.7$, $\Omega_m = 0.3$, $H_0 = 70 \text{ km s}^{-1} \text{ Mpc}^{-1}$.

2. THE UCSD SAMPLE

The UCSD sample consists of 68 objects selected from the 411 sources that comprise the complete Caltech-Jodrell Bank radio catalogs, including the Pearson-Readhead sample (PR), the Caltech-Jodrell Bank VLBI Surveys 1 and 2 (CJ1 and CJ2), and the Caltech-Jodrell Bank Flat-spectrum sample completion. While each sample was selected by a progressively lower flux density threshold, the sources for each sample were all selected to have declination (B1950) $\delta \geq 35^\circ$ and Galactic latitude $|b| \geq 10^\circ$. The PR sample includes 65 objects with flux density at 6 cm (4859 MHz), $S_{6cm} \geq 1.3 \text{ Jy}$ (Pearson & Readhead 1988). The CJ1 sample includes 135 sources with flux density at 6 cm, $1.3 \text{ Jy} \geq S_{6cm} \geq 0.7 \text{ Jy}$ (Polatidis et al. 1995; Thakkar et al. 1995; Xu et al. 1995), and the CJ2 sample consists of 193 mostly flat-spectrum objects with a flux density $S_{6cm} \geq 350 \text{ mJy}$ (Taylor et al. 1994; Henstock et al. 1995). The CJF (CJF; Taylor et al. 1996) is a compilation of the flat-spectrum radio sources (spectral index flatter than $\alpha_{1400\text{MHz}}^{4850\text{MHz}} \geq -0.5$) from the previous three surveys, plus and additional 18 sources for completion.

An optical campaign to determine the type of source, magnitude, and redshift of the radio catalog objects followed, the results of which were compiled in the CJ catalogs. The object optical identification and determination of the R magnitude was done by automated scanning of the POSS plates or by eye. Redshifts were primarily taken from Veron-Cetty, M.-P. & Veron, P. (1993) and from Henstock et al. (1997).

From this large radio sample, our selection criterion included all objects identified as quasars with $z_{em} > 2.0$ regardless of optical magnitude. The $z_{em} > 2.0$ cutoff was chosen to ensure sufficient spectral coverage to search for DLAs at wavelengths redward of the atmospheric cutoff at $\approx 3200\text{\AA}$. We also included in our sample of 68 objects all 14 sources designated as optical empty fields in order to be sure that we were not artificially selecting objects brighter than an arbitrary optical magnitude. And finally, we included the 5 sources for which there was a tentative optical identification, but no redshift information.

2.1. Observations and Analysis

Observations of most quasar candidate objects were first carried out at Palomar, with follow-up done at Keck for faint or “Empty Field” (EF) objects (see Table 1). The majority of our spectra have better than 6 \AA FWHM. Five of the 68 objects in our sample were previously observed at moderate spectral resolution and the data or results for these objects were taken from the literature. These included quasars Q0014+813, Q0201+365, Q0636+680, Q0642+449 which were observed by Sargent et al. (1989), and quasar Q1124+571 which was taken from Lanzetta et al. (1991). The N_{HI} measurement for the DLA towards Q0201+365 was taken from Lu et al. (1993).

Initial observations of most other targets were made

TABLE 1
DETAILS OF OBSERVATIONS

| Telescope | Date (No. nights) | Resolution (at 4000 Å) | No. of quasars observed |
|-----------|----------------------|---------------------------|----------------------------|
| Palomar | Nov 1995 (2) | 4-6 Å | 17 |
| Palomar | Apr 1996 (1) | 4-6 Å | 8 |
| Palomar | May 1996 (2) | 4-6 Å | 9 |
| Palomar | Dec 1996 (2) | 4-6 Å | 16 |
| Palomar | June 1997 (1) | 4-6 Å | 7 |
| Keck LRIS | Nov 2001 (1) | 4-6 Å | 3 |
| Keck ESI | Apr 2002 (1) | 0.5 Å | 14 |
| Keck ESI | Aug 2002 (1) | 0.5 Å | 7 |
| Keck LRIS | Dec 2002 (1) | 11 Å | 1 |
| Keck LRIS | May 2003 (1) | 3-5 Å | 14 |

with the 200-inch Hale telescope of the Palomar Observatory. Observations were made with the Double Spectrograph and utilized gratings that were 300 lines mm^{-1} in the blue and the 315 lines mm^{-1} in the red, resulting in 4-6 Å resolution using the 1" slit, and ≈ 10 Å resolution using the 2" slit when conditions were poor. All data were reduced using standard IRAF reduction packages.

Follow up observations of empty fields and faint quasars were done at Keck with the Echellette Spectrograph and Imager (ESI, Sheinis et al. 2002) and the Low Resolution Imaging Spectrometer (LRIS, Oke et al. 1995). With LRIS, the slit size was generally 0.7". The ESI observations utilized the 1.0" slit in LowD mode and the 0.5" slit in echellette mode.

Fifteen of the original 68 objects were excluded from the final statistical data set for the following reasons: Seven were determined to be galaxies, stars, or low redshift quasars, and the remaining eight were deemed empty fields (EFs). Table 2 contains the details of the final 53 quasars used in the UCSD statistics, while Table 3 and Table 4 contain a summary of the empty fields and the discarded objects respectively.

TABLE 4
DISCARDED OBJECTS

| Object | Reason for Discard | Survey |
|----------|----------------------------------|--------|
| 0843+575 | galaxy | CJ2 |
| 1125+596 | quasar at $z_{\text{em}} = 1.78$ | CJ2 |
| 1308+471 | galaxy | CJ2 |
| 1436+763 | star | CJ2 |
| 1809+568 | No significant emission feature | CJ2 |
| 2238+410 | Spectrum dubious | CJ2 |
| 2319+444 | quasar at $z_{\text{em}} = 1.24$ | CJ2 |

2.2. Damped $\text{Ly}\alpha$ systems

The Palomar data were reduced using standard IRAF packages, while the Keck data were reduced using IDL reduction software⁸. The reduced quasar spectra were continuum fitted and normalized and then analyzed to find regions in which the restframe equivalent width of an absorption feature was ≥ 5 Å and located in a region of good signal to noise. The equivalent width of the spectrum was calculated and an equivalent width array was then analyzed for regions that were greater than the 5 Å restframe

⁸<http://www.uchicago.edu/~xavier/IDL>

cutoff, as explained by Wolfe et al. (1995). We searched all regions of the spectrum blueward of $\text{Ly}\alpha$ emission, beginning with the lowest wavelength at which the error was below the restframe equivalent width threshold of ≥ 5 Å at the 5 σ level. All candidate detections were then inspected by eye to determine if they were indeed DLAs. False detections were usually quite obvious to exclude as blended lines, $\text{Ly}\beta$, etc.

Nine DLAs were found, two of which, towards quasars Q0824+355 and Q1014+615, were within 3,000 km s^{-1} of the $\text{Ly}\alpha$ emission peak, and therefore considered "associated". Following the standard practice, we exclude these "associated" DLAs from the sample in order to insure that we are not detecting objects that are physically associated with the quasar. Discarding these two leaves a final seven DLAs to be included in the UCSD sample.

2.2.1. $\text{Ly}\alpha$ Fits

The DLA systems were fitted with Voigt profiles using the IDL tool⁹ *x_fitdla* which allows the user to interactively modify the Voigt profile and continuum placement. In all but one case, that of Q1239+376, the DLA redshift was constrained by the corresponding metal lines with errors as given in Table 2. In the case of Q1239+376, the metal lines were too weak for use in constraining the DLA redshift and we instead determined the best fit interactively by eye using *x_fitdla*. This method results in larger uncertainties for z_{abs} and N_{HI} .

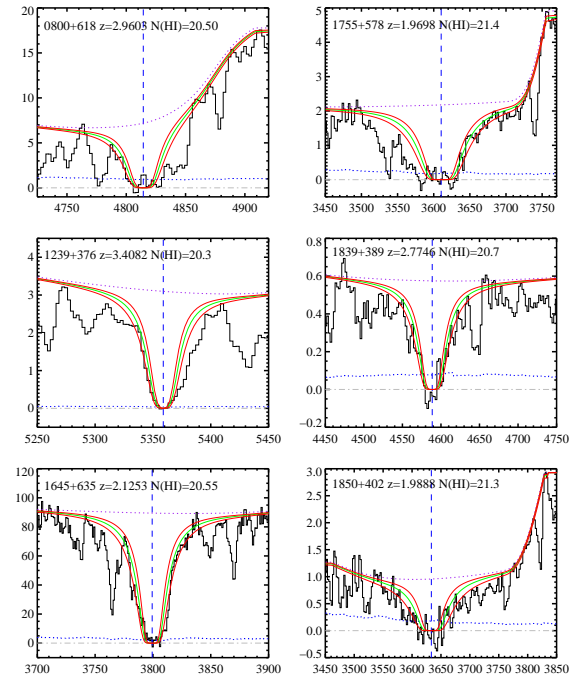


FIG. 1.— Voigt profile DLA fits for the six new DLA systems in the UCSD sample. The best Voigt profile is indicated by the green curve, surrounded by profiles with N_{HI} displacements ± 0.15 dex (or ± 0.25 dex) in red. The continuum placement can be seen as the purple dotted line, while the error array is represented by the blue dotted line.

For most of our sample DLAs a conservative estimate of the uncertainty in N_{HI} is 0.15 dex. However in one case,

⁹<http://www.uchicago.edu/~xavier/IDL>

TABLE 2
UCSD SURVEY SAMPLE

| Quasar | z_{em} | R mag | $N_{HI} \times 10^{20} \text{ cm}^{-2}$ | z_{abs} | z_{min} | z_{max} | 6cm Flux (Jy) | Survey ^d |
|-----------|----------|-------|---|---------------------|-----------|-----------|---------------|---------------------|
| Q0014+813 | 3.384 | 15.9 | ... | ... | 1.591 | 3.340 | 0.551 | CJ2 |
| Q0153+744 | 2.338 | 16.0 | ... | ... | 1.568 | 2.305 | 1.794 | PR |
| Q0201+365 | 2.912 | 17.5 | 2.4 ^a | 2.461 | 1.632 | 2.873 | 0.349 | CJ2 |
| Q0212+735 | 2.367 | 19.0 | ... | ... | 1.742 | 2.333 | 2.444 | PR |
| Q0604+728 | 3.53 | 20.3 | ... | ... | 2.651 | 3.485 | 0.654 | CJ2 |
| Q0609+607 | 2.710 | 19.0 | ... | ... | 1.650 | 2.673 | 1.059 | CJ2 |
| Q0620+389 | 3.470 | 20.0 | ... | ... | 1.842 | 3.425 | 0.87 | CJ1 |
| Q0627+532 | 2.200 | 18.5 | ... | ... | 1.619 | 2.168 | 0.485 | CJ2 |
| Q0636+680 | 3.174 | 16.2 | ... | ... | 1.591 | 3.132 | 0.499 | CJ2 |
| Q0642+449 | 3.406 | 18.5 | ... | ... | 1.591 | 3.362 | 0.78 | CJ1 |
| Q0727+409 | 2.501 | 17.0 | ... | ... | 1.578 | 2.466 | 0.468 | CJ2 |
| Q0738+491 | 2.318 | 21.0 | ... | ... | 1.928 | 2.285 | 0.352 | CJ2 |
| Q0749+426 | 3.590 | 18.1 | ... | ... | 2.118 | 3.544 | 0.461 | CJ2 |
| Q0800+618 | 3.04 | 19.6 | 3.16 ± 0.15 | 2.9603 ± 0.0017 | 2.234 | 3.000 | 0.981 | CJ2 |
| Q0803+452 | 2.102 | 19.6 | ... | ... | 1.594 | 2.071 | 0.414 | CJ2 |
| Q0824+355 | 2.249 | 19.7 | 2.0 ^b | 2.2433 | 1.655 | 2.217 | 0.746 | CJ2 |
| Q0833+585 | 2.101 | 18.0 | ... | ... | 1.546 | 2.070 | 1.11 | CJ1 |
| Q0836+710 | 2.180 | 16.5 | ... | ... | 1.507 | 2.148 | 2.423 | PR |
| Q0902+490 | 2.690 | 17.2 | ... | ... | 1.550 | 2.653 | 0.547 | CJ2 |
| Q0917+449 | 2.180 | 19.0 | ... | ... | 1.578 | 2.148 | 0.80 | CJ1 |
| Q0930+493 | 2.590 | 18.4 | ... | ... | 1.666 | 2.554 | 0.574 | CJ2 |
| Q1014+615 | 2.800 | 18.1 | 2.5 ^b | 2.7670 | 2.263 | 2.757 | 0.631 | CJ2 |
| Q1053+704 | 2.492 | 18.5 | ... | ... | 1.801 | 2.457 | 0.71 | CJ1 |
| Q1124+571 | 2.890 | 18.0 | ... | ... | 1.796 | 2.851 | 0.597 | CJ2 |
| Q1144+542 | 2.201 | 20.5 | ... | ... | 1.632 | 2.169 | 0.88 | CJ1 |
| Q1155+486 | 2.028 | 19.9 | ... | ... | 1.632 | 1.998 | 0.445 | CJ2 |
| Q1214+588 | 2.547 | 19.5 | ... | ... | 1.632 | 2.512 | 0.307 | CJ2 |
| Q1239+376 | 3.818 | 19.5 | 2.0 ± 0.15 | 3.4082 ^c | 2.344 | 3.770 | 0.446 | CJ2 |
| Q1325+436 | 2.073 | 18.5 | ... | ... | 1.549 | 2.042 | 0.533 | CJ2 |
| Q1333+459 | 2.449 | 18.5 | ... | ... | 1.612 | 2.414 | 0.76 | CJ1 |
| Q1337+637 | 2.558 | 18.5 | ... | ... | 1.550 | 2.522 | 0.431 | CJ2 |
| Q1413+373 | 2.360 | 17.3 | ... | ... | 1.607 | 2.326 | 0.383 | CJ2 |
| Q1421+482 | 2.220 | 18.9 | ... | ... | 1.549 | 2.188 | 0.536 | CJ2 |
| Q1427+543 | 2.980 | 20.7 | ... | ... | 2.331 | 2.940 | 0.718 | CJ2 |
| Q1435+638 | 2.068 | 15.0 | ... | ... | 1.591 | 2.037 | 1.24 | CJ1 |
| Q1526+670 | 3.020 | 17.1 | ... | ... | 1.977 | 2.980 | 0.417 | CJ2 |
| Q1547+507 | 2.169 | 18.5 | ... | ... | 1.582 | 2.137 | 0.74 | CJ1 |
| Q1602+576 | 2.858 | 16.8 | ... | ... | 1.630 | 2.819 | 0.351 | CJ2 |
| Q1624+416 | 2.550 | 22.0 | ... | ... | 1.732 | 2.515 | 1.632 | PR |
| Q1645+635 | 2.380 | 19.4 | 3.55 ± 0.15 | 2.1253 ± 0.0003 | 1.536 | 2.346 | 0.444 | CJ2 |
| Q1745+624 | 3.886 | 18.3 | ... | ... | 3.085 | 3.837 | 0.580 | CJ2 |
| Q1755+578 | 2.110 | 18.6 | 25.1 ± 0.15 | 1.9698 ± 0.0009 | 1.630 | 2.079 | 0.455 | CJ2 |
| Q1758+388 | 2.092 | 17.8 | ... | ... | 1.512 | 2.061 | 0.92 | CJ1 |
| Q1834+612 | 2.274 | 17.6 | ... | ... | 1.599 | 2.241 | 0.590 | CJ2 |
| Q1839+389 | 3.094 | 19.5 | 5.0 ± 0.15 | 2.7746 ± 0.0009 | 1.911 | 3.053 | 0.476 | CJ2 |
| Q1850+402 | 2.120 | 17.9 | 20.0 ± 0.25 | 1.9888 ± 0.0058 | 1.669 | 2.089 | 0.535 | CJ2 |
| Q2015+657 | 2.845 | 19.1 | ... | ... | 2.734 | 2.807 | 0.500 | CJ2 |
| Q2017+745 | 2.187 | 17.9 | ... | ... | 1.602 | 2.155 | 0.500 | CJ2 |
| Q2136+824 | 2.350 | 18.9 | ... | ... | 2.002 | 2.317 | 0.509 | CJ2 |
| Q2255+416 | 2.150 | 20.9 | ... | ... | 2.119 | 2.119 | 0.99 | CJ1 |
| Q2259+371 | 2.228 | 20.4 | ... | ... | 1.632 | 2.196 | 0.406 | CJ2 |
| Q2310+385 | 2.181 | 17.5 | ... | ... | 1.630 | 2.149 | 0.484 | CJ2 |
| Q2356+385 | 2.704 | 18.6 | ... | ... | 1.771 | 2.666 | 0.449 | CJ2 |

^a N_{HI} value taken from Lu et al. (1993).

^bAssociated systems: z_{abs} within $\approx 3,000 \text{ km s}^{-1}$ of z_{em} .

^cWeak metals, therefore best fit determined by eye.

^dCJ1, CJ2 = Caltech Jodrell Bank, PR = Pearson-Readhead

TABLE 3
EMPTY OR EXTENDED FIELDS

| Object | RA(J2000) | Dec(J2000) | Exp. time (s) | R_{lim}^a 3σ | Morphology | R mag ^b | 6cm Flux (Jy) | Survey |
|-----------------------|-------------|--------------|------------------|--------------------------|--------------------------------------|--------------------|--------------------|--------|
| 0102+480 | 01 05 49.93 | +48 19 03.19 | 294 | 26.1 | no detection | ... | 1.080 | CJ1 |
| 0633+596 | 06 38 02.87 | +59 33 22.21 | 500 | 26.4 | possibly extended | 25.8 ± 0.7 | 0.482 | CJ2 |
| 0718+793 | 07 26 11.74 | +79 11 31.0 | 500 | 26.1 | extended, $\approx 7'' \times 3''$ | 24.5 ± 0.4 | 0.467 ^c | CJ2 |
| 1107+607 | 11 10 13.09 | +60 28 42.57 | 600 | 26.5 | extended, $\approx 4'' \times 2.5''$ | 25.8 ± 0.8 | 0.400 | CJ2 |
| 1205+544 | 12 08 27.50 | +54 13 19.53 | 600 | 26.5 | possibly extended | 24.6 ± 0.3 | 0.397 | CJ2 |
| 1312+533 | 13 14 43.83 | +53 06 27.73 | 600 | 26.5 | extended, $\approx 3'' \times 3''$ | 25.4 ± 0.6 | 0.433 | CJ2 |
| 1828+399 | 18 29 56.52 | +39 57 34.69 | 900 | 26.9 | no detection | ... | 0.353 | CJ2 |
| 2054+611 ^d | 20 55 38.84 | +61 22 00.64 | 900 | 26.7 | possibly extended | ... | 0.414 | CJ2 |

^a Limiting magnitude per seeing element above sky background

^b R mag estimation of extended smudge

^c @1.4GHz

^d Uncertain identification, either $z = 1.588, 3.0, 3.3$

that of Q1850+402, where the Voigt profile proved difficult to fit, we report an uncertainty of 0.25 dex in N_{HI} . Figure 1 shows Voigt profile fits for each DLA, except for the $z_{abs} = 2.461$ DLA towards Q0201+365, which is in the existing literature (Sargent et al. 1989). Now we will give brief details on each DLA system.

Q0201+365: N_{HI} fit taken from Lu et al. (1993) and discussion therein.

Q0800+618: The difficulty in estimating the continuum placement in such close proximity to the Ly α emission peak made this DLA system somewhat difficult to fit. There is also a possibility of some blended absorption.

Q1239+376: High signal to noise and good placement. The only problem with this fit was some blending on the red side.

Q1645+635: High signal to noise and lack of blending resulted in a good Voigt profile fit to this DLA profile.

Q1755+578: Close proximity to Ly α emission peak and blending on the blueward side made the fit difficult.

Q1839+389: Straightforward fit and good continuum.

Q1850+402: Close proximity to Ly α emission peak, lower signal to noise and blending made this a more difficult fit, yielding an increased error margin on the Voigt profile of 0.25 dex.

3. DLA STATISTICS

Our goal of determining the impact of dust obscuration in surveys of DLAs requires that we be able to compare our radio-selected survey to the results of optically-selected surveys. We will now introduce some of the standard statistical quantities used to describe and quantify surveys of DLAs.

3.1. Δz , $g(z)$ and $n(z)$

The redshift path, Δz , is defined as the total redshift interval along which a damped Ly α feature with rest frame equivalent width exceeding 5Å would be detected at more than 5σ significance. It is defined as follows,

$$\Delta z = \sum_{i=1}^n (z_i^{max} - z_i^{min}) \quad (1)$$

where the summation is over the n quasars in the survey, z_{min} is determined to be the lowest spectral wavelength with good signal-to-noise, and z_{max} is the redshift corresponding to the maximum spectral wavelength included in the search. We define z_{max} by,

$$z_{max} \equiv z_{qso} - (1 + z_{qso})/100 \quad (2)$$

This corresponds to 3000 km s⁻¹ blueward of the Ly α emission feature. This cutoff ensures that a damped Ly α system is not physically associated with the quasar.

The redshift path density, $g(z)$, gives an idea of the statistical significance as a function of redshift of a survey for DLAs. It is defined as the number of quasars with sight-lines containing a particular redshift interval (Lanzetta et al. 1991). Specifically,

$$g(z) = \sum_{i=1}^n H(z_i^{max} - z) H(z - z_i^{min}) \quad (3)$$

where H is the Heaviside step function, the sum is over n quasars (Lanzetta et al. 1991) and,

$$\Delta z = \int g(z) dz \quad (4)$$

where the integral is over all z paths in the survey. The DLA number density, $n(z)$, is simply the number of DLAs per unit redshift,

$$n(z) = \frac{m}{\Delta z} \quad (5)$$

where m is the number of DLAs.

3.2. $f_{HI}(N, X)$: The $H I$ Frequency Distribution Function

Following the direction of previous works such as Lanzetta et al. (1991) and PHW05, we can define a neutral hydrogen

frequency distribution function that describes the number of DLAs in a range of column densities, $(N, N + dN)$, and a range of absorption distances, $(X, X + dX)$,

$$f_{\text{HI}}(N, X) dN dX, \quad (6)$$

where the absorption distance, ΔX , is defined as follows:

$$\Delta X = \int dX \equiv \int \frac{H_0}{H(z)} (1+z)^2 dz \quad (7)$$

where H_0 is Hubble's constant.

3.3. $\ell_{\text{DLA}}(X)$: The Damped Ly α Line Density

The zeroth moment of the H I frequency distribution function is known as the line-density of DLAs $\ell_{\text{DLA}}(X)$. The line-density represents the number of systems per unit absorption distance and is defined as:

$$\ell_{\text{DLA}}(X) = \int_{N_t}^{\infty} f_{\text{HI}}(N, X) dN. \quad (8)$$

As described in PHW05, the line-density is related to the covering fraction of DLAs on the sky. This relationship is apparent if we describe the frequency distribution function in terms of an average cross-section $A(X)$, and the comoving number density of DLAs $n_{\text{DLA}}(X)$:

$$f_{\text{HI}}(N, X) \equiv (c/H_0) n_{\text{DLA}}(X) A(X). \quad (9)$$

(see Wolfe, Gawiser, & Prochaska 2005, for details).

3.4. Ω_g : The Cosmological Neutral Gas Mass Density

An important parameter in describing any quasar survey for DLAs is the first moment of the H I frequency distribution function, the neutral gas mass density, Ω_g . It is believed that Ω_g is closely related to the amount of neutral hydrogen available for star formation and hence, places an important tracer on the history of star formation in the Universe. Acquiring this parameter through surveys for DLAs is an important constraint on the neutral gas reservoir available for star formation in the early ($z > 2$) Universe. Ω_g is defined as follows:

$$\Omega_g(X) \equiv \frac{\mu m_H H_0}{c \rho_c} \int_{N_{\min}}^{N_{\max}} N f_{\text{HI}}(N, X) dN \quad (10)$$

where μ is the mean molecular mass of the gas (taken to be 1.3), m_H is the mass of the hydrogen atom, ρ_c is the critical mass density, $f_{\text{HI}}(N, X)$ is the frequency distribution function of neutral gas found in DLAs and the integration is from $N_{\min} = 2 \times 10^{20} \text{ cm}^{-2}$ to $N_{\max} = \infty$. We follow previous works, i.e. Lanzetta et al. (1991), and replace this frequency distribution function by its evaluation in the discrete limit as follows,

$$\Omega_g = \frac{\mu m_H H_0}{c \rho_c} \frac{\sum N(\text{HI})}{\Delta X}, \quad (11)$$

where the sum is performed over the N_{HI} measurements of the DLA systems in a given redshift interval with total pathlength ΔX . As emphasized by PHW05 and discussed

below, equation 11 only provides an accurate evaluation of equation 10 if the survey is sufficiently large that the observed $f_{\text{HI}}(N, X)$ distribution becomes steeper than N^{-2} at large N_{HI} . If this is not the case, equation 11 provides only a lower limit to Ω_g .

4. RESULTS

We will now describe the results of the UCSD radio-selected survey, the CORALS radio-selected survey, and the combination of these two surveys, which we will refer to as the combined sample. Details of the results of each survey are listed in Table 5.

4.1. UCSD Survey Results

The UCSD sample consists of 7 DLAs in 53 quasars of $z_{\text{em}} \geq 2.0$ with a total redshift path of $\Delta z = 41.15$. This resulted in a number of DLAs per unit redshift, $n(z) = 0.17^{+0.08}_{-0.07}$, where the error bars are the standard 1σ Poissonian errors using Gehrels' tables for small number statistics (Gehrels 1986). Figure 2 presents $g(z)$ versus z for the UCSD sample in green. The line density of DLAs over the cosmological redshift path of $\Delta X = 130.43$ resulted in $\ell_{\text{DLA}}(X) = 0.05^{+0.03}_{-0.02}$, while the mass density of neutral gas is $\Omega_g = 0.84^{+0.43}_{-0.45} \times 10^{-3}$. While we report Ω_g as a detection, it is strictly speaking, a lower limit because we do not measure $f_{\text{HI}}(N, X)$ to fall off faster than N^{-2} (see § 4.3).

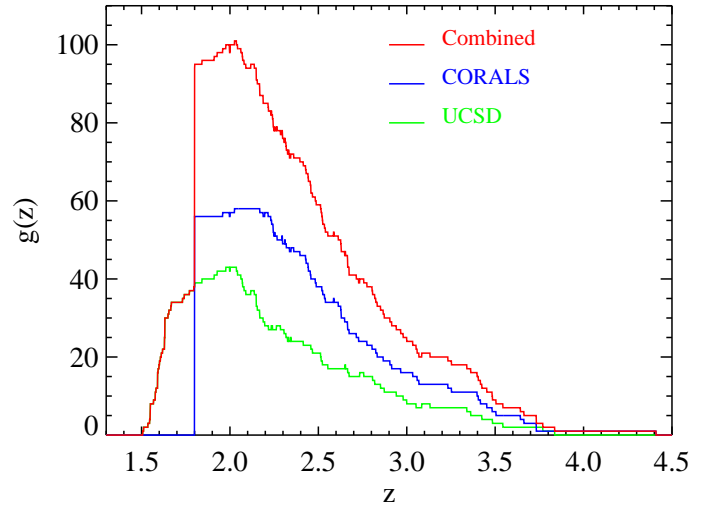


FIG. 2.— Redshift sensitivity function $g(z)$ as a function of redshift for the UCSD survey, the CORALS survey, and the combined sample.

4.2. CORALS Survey Results

The Complete Optical and Radio Absorption Line Survey (CORALS) (Ellison et al. 2001) was the first attempt to utilize a radio-selected quasar survey as a basis for a search for DLAs. They selected quasars from the complete Parkes quarter-Jansky flat spectrum sample (Jackson et al. 2002), comprised of 878 radio sources with spectral index $\alpha_{2.7\text{GHz}}^{5\text{GHz}} > -0.4$ and declinations between $+2.5^\circ$ and -80° . Ellison et al. (2001) limited their data set to 66

$z_{em} \geq 2.2$ quasars in which they found 22 DLAs. Three of these DLAs were classified as “associated” and dropped from the final sample. Two more DLAs were excluded because they fell outside of the range $1.8 \leq z_{abs} \leq 3.5$, that Ellison et al. (2001) set for their statistical sample, citing that there appears to be little evolution of Ω_g in this range. Since the UCSD sample did not have this z_{abs}^{max} cutoff, we included all 19 CORALS DLAs in the statistics for the combined sample.

Detailed results of the CORALS survey, including the two DLAs in sightlines to quasars with $z_{abs} > 3.5$, are listed in Table 5. Statistics for the number density and neutral gas mass density in the CORALS survey resulted in their conclusion that previous, magnitude limited surveys could have underestimated these values by as much as a factor of two. The plot of $g(z)$ versus z for the CORALS survey is shown in blue in Figure 2. Over a total redshift interval, $\Delta z = 57.16$, the number of DLAs per unit redshift, $n(z) = 0.33^{+0.10}_{-0.07}$. Over a cosmological redshift path of $\Delta X = 186.68$, the line density of DLAs in the CORALS survey, $\ell_{DLA}(X) = 0.102^{+0.03}_{-0.02}$, which is double that of the UCSD survey. CORALS compared their neutral gas mass density in DLAs $\Omega_g = 1.37^{+0.53}_{-0.55} \times 10^{-3}$ with the compilation of Péroux et al. (2001) and Rao & Turnshek (2000), and concluded that Ω_g derived from optically-selected surveys could be underestimated by up to a factor of two.

However, Ellison et al. do concede the uncertainty of their conclusion primarily because the small survey fails to fully sample the column density distribution and secondly because their high value of Ω_g is dominated by two relatively high column density systems (both incidentally in front of “moderately bright” quasars, $B = 19.5, 20$, which qualitatively matches the result of PHW05 that there is an anti-correlation between quasar magnitude and N_{HI}).

TABLE 5
RESULTS

| feature | UCSD | CORALS | COMBINED |
|--|------------------------|------------------------|------------------------|
| No. quasars | 53 | 66 | 119 |
| No. DLAs | 7 | 19 | 26 |
| Δz | 41.15 | 57.16 | 98.31 |
| $n(z)$ | $0.17^{+0.08}_{-0.07}$ | $0.33^{+0.10}_{-0.07}$ | $0.26^{+0.06}_{-0.05}$ |
| $\ell_{DLA}(X)$ | $0.05^{+0.03}_{-0.02}$ | $0.10^{+0.03}_{-0.02}$ | $0.08^{+0.02}_{-0.02}$ |
| $\langle N_{HI} \rangle \text{ cm}^{-2}$ | 8.744×10^{20} | 7.532×10^{20} | 7.858×10^{20} |
| $\langle z \rangle$ | 2.53 | 2.50 | 2.51 |
| $\langle z \rangle_{weighted}$ | 2.17 | 2.33 | 2.28 |
| $\Sigma N_{HI} \text{ cm}^{-2}$ | 0.61×10^{22} | 1.43×10^{22} | 2.04×10^{22} |
| ΔX | 130.43 | 186.68 | 317.11 |
| $\Omega_g (\times 10^{-3})$ | $0.84^{+0.43}_{-0.45}$ | $1.37^{+0.53}_{-0.55}$ | $1.15^{+0.37}_{-0.38}$ |
| Error | $\pm 54\%$ | $\pm 41\%$ | $\pm 33\%$ |

4.3. Combined Results

For simplicity, we present detailed analyses for just the combined sample, which has the greatest statistical significance. Figure 2 presents $g(z)$ versus z for the combined sample in red. The CORALS sample begins abruptly at $z = 1.8$, the z_{min} cutoff of their sample. The UCSD sample continues down to a $z_{min} \approx 1.51$ for some quasars. For $z \approx 2$ the combined sample is nearly double that of CORALS. For higher redshift intervals (i.e. $z = 3$), the CORALS survey contributes roughly 2/3 of the path-length. Of course, the combined sample gives the best constrained estimate of the number density of $n(z) = 0.26^{+0.06}_{-0.05}$.

The combined sample is large enough to attempt an analysis of the H I distribution function, $f_{HI}(N, X)$. This sample spans the redshift interval $z = [1.51, 4.4]$ with an integrated absorption pathlength $\Delta X = 317.11$ and a column density weighted mean redshift of 2.28. In practice, we can evaluate $f_{HI}(N, X)$ in the discrete limit and plot the resulting $f_{HI}(N, X)$ in N_{HI} bins of some ΔN . In Figure 3, we plot in red $f_{HI}(N, X)$ for the combined sample, in N_{HI} bins of $\Delta N = 0.4 \text{ dex}$, calculated in the following way:

$$f_{HI}(N, X) = \frac{m_{DLA}(N, N + \Delta N)}{\Delta X}, \quad (12)$$

where m_{DLA} is the number of damped Ly α systems within $(N, N + \Delta N)$ in the ΔX interval and the error bars are determined by Poisson uncertainty at the 84% c.l. according to the value of m_{DLA} . Also plotted, in black, are the results of the optically-selected SDSS-DR3 (PHW05) survey for comparison. Following PHW05, we have overplotted the best-fit solutions of two possible functional forms of $f_{HI}(N, X)$. Because of the small sample size of this survey we will attempt to fit only a single power-law and a Γ -function. The single power-law form is as follows:

$$f_{HI}(N, X) = k_1 N^{\alpha_1}, \quad (13)$$

and the Γ -function is (e.g. Fall & Pei 1993):

$$f_{HI}(N, X) = k_2 \left(\frac{N}{N_\gamma} \right)^{\alpha_2} \exp \left(\frac{-N}{N_\gamma} \right). \quad (14)$$

We have performed a maximum likelihood analysis to constrain the parameters and set the constants k_1 and k_2 . A summary of the fit parameters, along with those of the optically-selected SDSS-DR3 survey for comparison, is given in Table 6. The best fit slope of the single power-law is $\alpha_1 = -2.18^{+0.20}_{-0.26}$. This single power-law slope can be compared favorably with the optical SDSS-DR3 survey single power-law slope of $\alpha_1 = -2.19^{+0.05}_{-0.05}$ over their entire redshift range, $z = [2.2, 5.5]$. This correspondence is expected because the radio-selected survey is dominated by the low column density end which matches that of the optical, and can be seen as a confirmation of the two techniques.

While the single-power law gives a good fit to the radio-selected data, we also attempt to fit the Γ -function for the following two reasons: First, the single-power law is unphysical, i.e. the fit must turn over in order for Ω_g to converge, and second, unlike the single-power law, the Γ -function provided a satisfactory fit to the optically-selected data. However, unlike the optically-selected sample, the radio-selected sample gives nearly the same fit for the Γ -function as for the single power-law, $\alpha_2 = -2.12^{+0.22}_{-0.27}$. While we derive a formal value of the break column density $N_\gamma = 22.49^{+0.29}_{-0.36}$, we interpret this as an unrealistic extrapolation of the data. Rather, the small size of the radio-selected sample cannot reliably determine a break column density, and therefore we cannot demonstrate that our Ω_g converges.

To determine if the radio-selected data rules out the optically-selected Γ -function fit, we performed a chi-squared test on the radio-selected data and optically-selected Γ -function fit. The results of the chi-squared test, $\text{Prob}_1(\chi^2)$

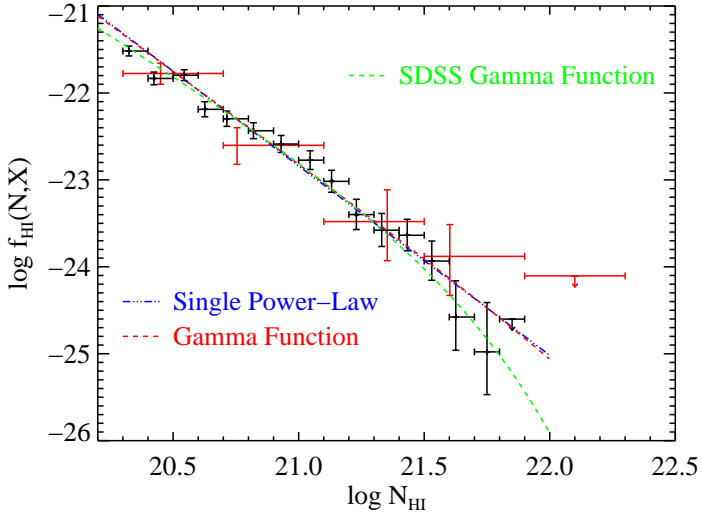


FIG. 3.— The H I frequency distribution $f_{\text{HI}}(N, X)$ for the 26 DLAs of the combined sample is plotted in red. Overplotted are the fits of a single power-law, the dot-dashed line in blue, and a Γ -function, the dashed line in red. The last bin contains the 2σ upper limit. Plotted in black is the $f_{\text{HI}}(N, X)$ for the optical data from the SDSS-DR3, with the Γ -function fit in green.

$> 5.96) = 1.5\%$ show that we can reject the fit at the 5% level, but not at the 1% level of confidence. While this may be evidence for modest disagreement between the two samples, we interpret this disagreement to be primarily due to the fact that we cannot constrain the radio-selected fit at large N_{HI} , i.e. the radio-selected sample does not contain enough DLAs to fully sample the H I distribution function. We note that a more conservative two-sided KS test shows agreement between the radio-selected data and the optically-selected Γ -function fit at the 77% level.

TABLE 6
FITS TO $f_{\text{HI}}(N, X)$

| Form | Parameters | SDSS-DR3 Optical ^{a, o} | Combined Radio ^c |
|--------|-----------------|----------------------------------|-----------------------------|
| Single | $\log k_1$ | 23.36 | 22.90 |
| | α_1 | $-2.19^{+0.05}_{-0.05}$ | $-2.18^{+0.20}_{-0.26}$ |
| Gamma | $\log k_2$ | $-23.52^{+0.02}_{-0.02}$ | $-25.97^{+0.09}_{-0.08}$ |
| | $\log N_\gamma$ | $21.48^{+0.07}_{-0.10}$ | $22.49^{+0.29}_{-0.36}$ |
| | α_2 | $-1.80^{+0.06}_{-0.06}$ | $-2.12^{+0.22}_{-0.27}$ |

^aProchaska, Herbert-Fort, & Wolfe (2005)

^bMean absorption redshift = 3.06

^cMean absorption redshift = 2.28

The line density of DLAs in the combined sample, taken over the entire redshift interval, $z = [1.5, 4.4]$, is $\ell_{\text{DLA}}(X) = 0.08^{+0.02}_{-0.02}$ at a median $z = 2.35$, where the errors represent the 1σ Poisson uncertainty in m_{DLA} . In Figure 4 we plot $\ell_{\text{DLA}}(X)$ for the combined sample in red, evaluated in the discrete limit,

$$\ell_{\text{DLA}}(X) = \frac{m_{\text{DLA}}}{\Delta X} \quad (15)$$

We have grouped the data into four redshift bins, $z = [1.5,$

2.2], [2.2, 2.5], [2.5, 3.0], and [3.0, 4.4] to allow for comparison with the results of PHW05. We have overplotted the results of the SDSS-DR3 optical survey in black. These points are grouped into redshift bins $z = [2.2, 2.5]$, [2.5, 3.0], [3.0, 3.5], [3.5, 4.0], [4.0, 5.3]. The black point marked by a star in redshift bin $z = [1.5, 2.2]$ is a compilation of optical surveys for DLAs produced by Péroux et al. (2003). Although the central values of the line densities of the radio and optically-selected surveys are different, the difference is not statistically significant. Note the radio sample gives a somewhat higher line density at all redshifts, and it is interesting to note that beginning at $z = 2.2$, the trend of increasing line density with increasing redshift, $z > 2.2$, is present in both samples. In fact, the central values of the radio sample follow the same qualitative shape, even the unusual ‘dip’ at $z \approx 2.3$. While it would make sense that the SDSS-DR3 survey, with its statistically significant numbers of quasars and DLAs is actually detecting a physically meaningful trend – PHW05 claim the decline in $\ell_{\text{DLA}}(X)$ is due to a decrease in DLA cross-section with time – the correspondence with the combined radio sample, of relatively so few objects, is likely a coincidence. However, although the error bars are large, we can interpret this similarity in line density evolution with the statistically significant results of the SDSS-DR3 as support of our results.

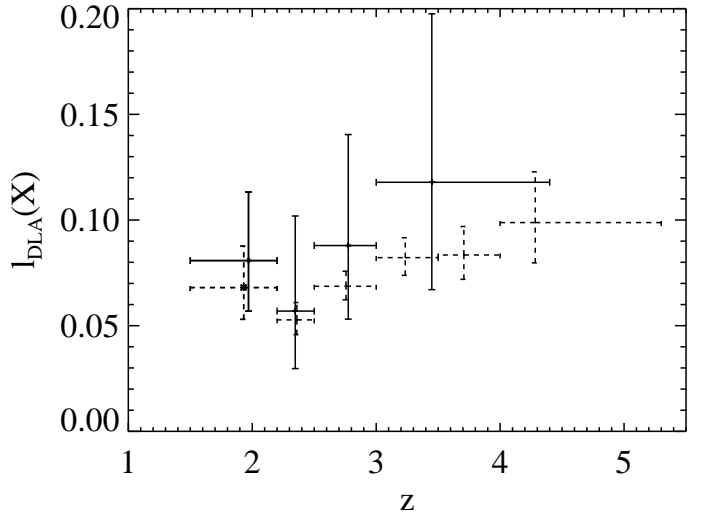


FIG. 4.— Plot of the line density of DLA systems $\ell_{\text{DLA}}(X)$ versus redshift for the combined sample (solid lines). Overplotted is the $\ell_{\text{DLA}}(X)$ for the optical data from the SDSS-DR3 survey and the Péroux compilation (dashed lines).

While we report a detection of the neutral gas mass density, $\Omega_g = 1.15^{+0.37}_{-0.38} \times 10^{-3}$, our result is actually a lower limit due to the insufficient size of the combined sample. In Figure 5 we plot Ω_g for each of the UCSD, CORALS and combined samples. Errors are calculated using a modified bootstrap method as described by PHW05, and the values are plotted at the N_{HI} weighted mean redshift. Also plotted, in black, are the Ω_g values determined by the optically-selected SDSS-DR3 survey (PHW05), which covers a redshift range $z \geq 2.2$. Because the SDSS-DR3 sample consists of over 500 DLAs the values of Ω_g are plotted in five redshift bins: $z = [2.2, 2.5]$, [2.5, 3.0], [3.0, 3.5], [3.5,

4.0], and [4.0, 5.5]. And finally, plotted in the bin range $z = [1.7, 2.2]$, is the compilation by Péroux et al. (2003). It is seen that the lower limits of all of the radio-selected samples agree well with the optically-selected data.

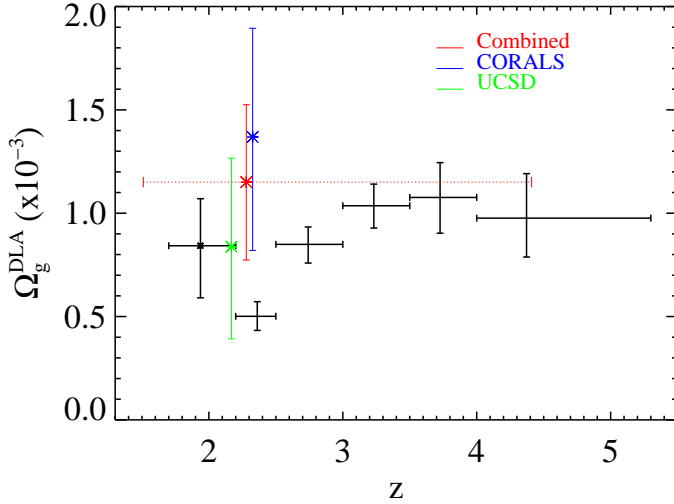


FIG. 5.— The neutral gas mass density, Ω_g , of the UCSD, CORALS and combined samples are plotted in green, blue and red respectively. For clarity, only the redshift bin of the combined sample is plotted, $z_{\text{combined}} = [1.51, 4.41]$ (dotted red). The redshift bins of the radio samples (not plotted) are $z_{\text{ucsd}} = [1.51, 3.84]$, and $z_{\text{corals}} = [1.80, 4.41]$ and the points are plotted at the N_{HI} weighted mean redshift. Also plotted are the values of Ω_g as a function of redshift for the optical SDSS-DR3 survey (black points). The Péroux compilation data point at $z < 2.2$ (marked with a cross) does not include measurements from the SDSS survey. All error bars are 1σ .

4.4. Empty Fields

The eight fields for which no optical identification of a quasar was obtained are called the “Empty Fields” (EFs). Table 3 contains the details of each EF while Figure 6 contains Keck images of the EFs. These eight fields were determined to contain either nothing of significance, or merely a faint extended smudge when imaged with Keck in the R band for ≈ 600 seconds. In either case, it was not possible to obtain spectra. While all of the previous analyses in this paper were conducted as if these fields did not exist, we actually must determine a method of including them in the sample in order for our survey to be considered complete. Assuming that the fields were truly empty, i.e. the optical source was fainter than our magnitude limit on Keck, and that pointing errors or some other experimental errors did not result in radio-source misidentification, we can make two extreme, simplifying assumptions. On the one hand, we can assume that no DLAs are present toward these optically faint quasars and calculate a lower limit on Ω_g by including some average redshift path length for each object, where the average pathlength is determined from the known quasars in our survey. On the other extreme we can assume that each EF is actually empty because of the presence of a high column density, dusty DLA. We can assume that each EF contains an average to high column-density DLA and estimate an upper limit on Ω_g .

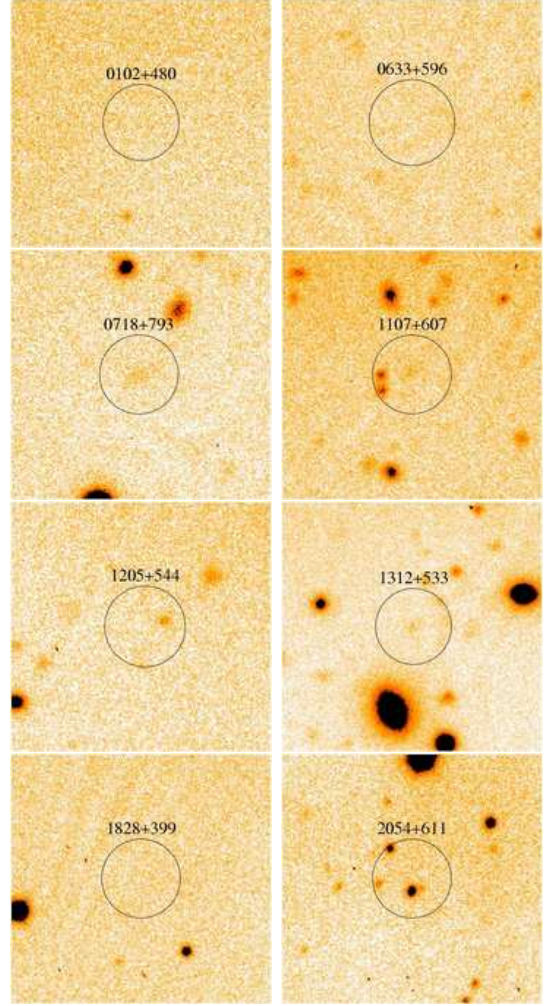


FIG. 6.— R band images of the empty or extended fields. Exposure times are given in Table 3. The circle radius is ≈ 5 arcsec. All image orientations are the standard North (up), East (left).

Using the results of the combined sample, we determine the average redshift path per quasar to be $\langle \Delta X \rangle = 2.66$. Assuming that each of the eight EFs would contribute this amount of redshift path gives a new total redshift path searched of $\Delta X = 338.43$. The lower limit on Ω_g , assuming that none of the EFs contained a DLA, is $\Omega_g^{\text{lower}} = 1.08 \times 10^{-3}$. The upper limit, assuming that each of the EFs contains a DLA of average column density in our survey, $N_{\text{HI}} = 7.86 \times 10^{20} \text{ cm}^{-2}$, results in an upper limit of $\Omega_g^{\text{upper}} = 1.41 \times 10^{-3}$. While both the lower and upper limit on Ω_g , derived by including the EFs, are clearly within the error of the combined value of $\Omega_g = 1.15^{+0.37}_{-0.38} \times 10^{-3}$, it is notable that the upper limit is only $\approx 22\%$ larger than Ω_g , i.e. even if each EF contains a dusty DLA of our average N_{HI} , the effect on Ω_g would be relatively small.

We can take the analysis one step further and allow the average value of N_{HI} to exceed $7.86 \times 10^{20} \text{ cm}^{-2}$. To determine the minimum average column density DLA that would affect our results we assume that each EF contains a quasar at our average redshift and a DLA of fixed column density which we vary from the lower limit, $N_{\text{HI}} =$

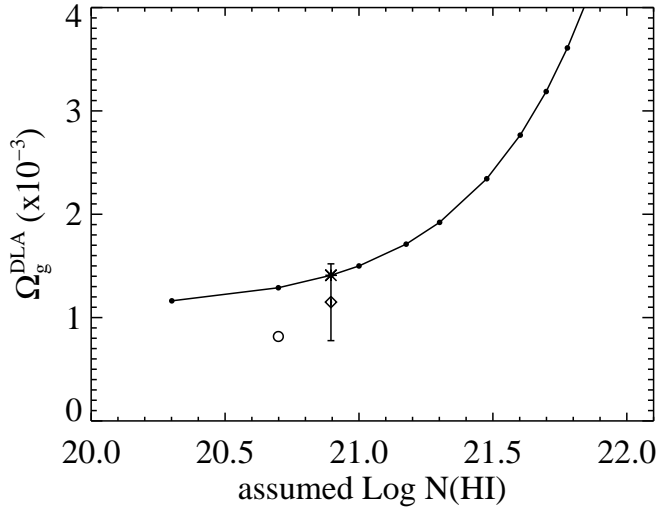


FIG. 7.— This figure demonstrates the potential impact that the empty fields could have on Ω_g , the neutral gas mass density. We calculate the resultant value of Ω_g assuming that each of the eight empty fields contains a DLA of the stated N_{HI} . The diamond with 1σ error bars is the value of Ω_g found from the combined radio sample, calculated by ignoring the empty fields. The asterisk represents the value of Ω_g if each of the empty fields contained a DLA of our average $N_{\text{HI}} = 7.86 \times 10^{20} \text{ cm}^{-2}$. For reference, the optically selected SDSS survey value is plotted as an unfilled circle.

$2 \times 10^{20} \text{ cm}^{-2}$, to the generally observed highest column densities of $N_{\text{HI}} \approx 1 \times 10^{22} \text{ cm}^{-2}$. We plot the results in Figure 7.

As previously stated, if we assume that each EF contains a DLA of average column density in our survey, $N_{\text{HI}} = 7.86 \times 10^{20} \text{ cm}^{-2}$, we derive an $\Omega_g = 1.41 \times 10^{-3}$, indicated in Figure 7 by the blue asterisk. Compare this with the red point and error bar, our radio-selected survey value of Ω_g , derived by ignoring the EFs. For reference, the optically selected SDSS-DR3 survey, at $\Omega_g = 0.82^{+0.05}_{-0.05} \times 10^{-3}$, is plotted in green. From Figure 7 it is seen that if each EF contained a DLA of $N_{\text{HI}} \approx 10^{21.2} \text{ cm}^{-2}$ or larger, a relatively large value occurring in only $\approx 15\%$ of our sample, the impact of the EFs would be large enough to increase the resultant value of Ω_g by $\approx 50\%$.

There are, however, several arguments for why these EFs are most likely *not* $z_{\text{em}} > 2$ quasars extinguished by very dusty, high column density DLAs. If we extrapolate the H I frequency distribution function, $f_{\text{HI}}(N, X)$ resulting from the radio-selected sample, as seen in Figure 3, we would expect not more than 1 DLA with $N_{\text{HI}} > 10^{22} \text{ cm}^{-2}$. If two or more high column density systems existed, the resulting $f_{\text{HI}}(N, X)$ would be unphysical assuming galaxies have declining surface density profiles. In this case, we would require a bimodal population consisting of high column density, high dust-to-gas ratio systems, such as molecular clouds, that would be missed in optical surveys.

While we cannot rule out the existence of a bimodal population, we can determine exactly how many high column density systems the current radio-selected distribution function would predict. We plot the cumulative number of DLAs above a certain minimum H I column density and extrapolate using our single power-law fit. From this plot, in Figure 8, it is apparent that we would expect only

0.3 DLAs with $N_{\text{HI}} > 10^{22} \text{ cm}^{-2}$. Additionally, in the case of the five fields containing faint extended emission, we can use scaling arguments to show that if we assume this emission is actually the resolved quasar host galaxy, then the quasar would have to be a low redshift object and would not have been included in our $z_{\text{em}} > 2.0$ survey. Adopting the typical high- z quasar host galaxy scale length of $\approx 12 \text{ kpc}$ (Kuhlbrot et al. 2005), we can estimate the angular size at $z = 2.0$ to be $\approx 1.4 \text{ arcsec}$. Careful inspection of the extended fields reveals extended blobs on the order of 3 arcsec or larger, making these low z quasars that would not have been included in our survey.

In an effort to determine the nature of the EFs, we are currently conducting an observing program on the Green Bank Telescope (GBT) to search for 21 cm absorption along the sightlines to these EFs. We will carry out a redshift path search from $z = [0.5, 3.9]$ using the frequencies of $\approx 300 \text{ MHz} - 900 \text{ MHz}$. If a high column density, dusty system does exist along the line of sight and is blocking out the quasar light, it is likely that we will detect it in absorption.

5. ANALYSIS & DISCUSSION

The best way of determining the significance of dust obscuration of quasars is to compare the results of magnitude limited and radio-selected quasar surveys for DLAs. The primary problem with this method has so far been the limited survey size of the radio-selected surveys and the resultant large error bars that preclude conclusive results. While the UCSD survey itself was slightly smaller than the previously published CORALS survey, combining the two surveys in effect doubles the size. However, the uncertainties of the combined sample, whose size is still more than an order of magnitude smaller than the current optical samples, are so large that definitive statements remain elusive.

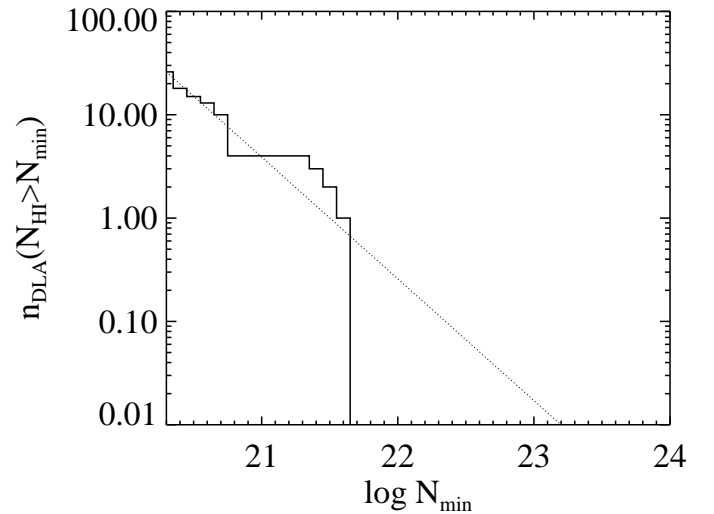


FIG. 8.— The cumulative distribution of the number of DLAs with a specific minimum N_{HI} . Overplotted is the single power-law fit to the distribution function (dotted line). It is seen that only 0.3 DLAs are expected with $N_{\text{HI}} > 10^{22} \text{ cm}^{-2}$.

To make a simple estimate of the number of radio selected DLAs necessary to conclusively answer the ques-

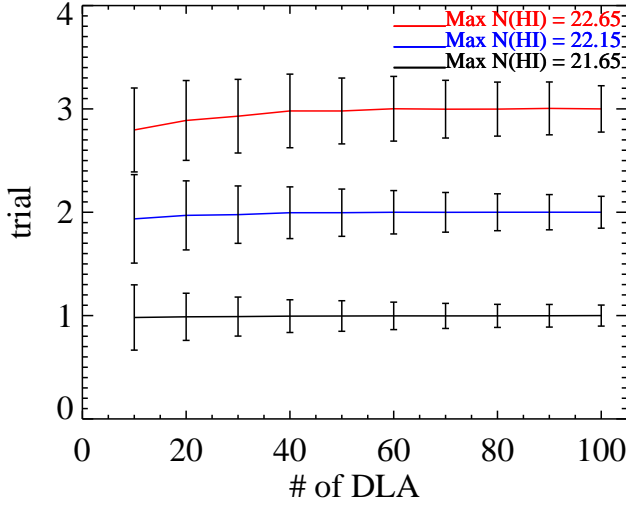


FIG. 9.— The results of bootstrapping error on samples of the given number of DLAs with maximum column densities of $N_{\text{HI}} = 10^{21.65} \text{ cm}^{-2}$ (to match the combined sample), the black line, $N_{\text{HI}} = 10^{22.15} \text{ cm}^{-2}$, the blue line, and $N_{\text{HI}} = 10^{22.65} \text{ cm}^{-2}$, the red line. It is seen that a sample with maximum $N_{\text{HI}} = 10^{21.65} \text{ cm}^{-2}$, will give an error in the desired range of $\pm 10\%$ at ≈ 100 DLAs.

tion of dust bias, we performed the following analysis. If we desire a result with errors of no larger than $\approx 10\%$, we can perform a bootstrap error evaluation on a random sample of DLAs each time increasing the number of DLAs to determine how many DLAs are necessary to give the desired precision. In Figure 9 we plot the results of our bootstrap error estimation, normalized to one and offset for each different sample type. The estimation was performed on random N_{HI} samples with minimum $N_{\text{HI}} = 10^{20.3} \text{ cm}^{-2}$, and three different maximum column densities, $N_{\text{HI}} = 10^{21.65} \text{ cm}^{-2}$, to match the upper limit of the combined radio sample, $N_{\text{HI}} = 10^{22.15} \text{ cm}^{-2}$, and $N_{\text{HI}} = 10^{22.65} \text{ cm}^{-2}$. It can be seen that in a sample with a maximum column density similar to the combined sample, the desired $\approx 10\%$ error is achieved with a sample of ≈ 100 DLAs. As the maximum column density is increased, the error bars increase as well. Note that the bootstrap errors of our actual sample (number of DLAs = 26, error $\approx 30\%$) are slightly bigger than those of the randomly generated samples due to the fact that our sample contains only a few high column density systems.

To definitively answer the question of dust bias we would ideally hope to at least approach the total redshift path searched by optical surveys in order to make valid comparisons. In the combined radio-selected sample, the total cosmological redshift path searched was $\Delta X = 317.11$. Compared with the total redshift path surveyed by the latest large optical survey, SDSS-DR3 with $\Delta X = 7333.2$, we are still more than an order of magnitude smaller.

The combined radio-selected central value of Ω_g is slightly higher than all of the optically-selected values, as plotted in Figure 5. However, when considering the 1σ lower limits of the radio-selected values of Ω_g , no difference between the magnitude-limited sample and the radio-selected samples can be ascertained. If we ignore the possibility of evolution in Ω_g we can compare the entire SDSS-DR3

optically-selected survey over the complete redshift range with the radio-selected value. Excluding the Péroux point, the SDSS-DR3 value taken over one redshift bin, $z = [2.2, 5.5]$, gives $\Omega_g = 0.82^{+0.05}_{-0.05} \times 10^{-3}$. Comparing this value with the 1σ lower limit of the combined radio-selected value of $\Omega_g^{\text{low}} = 0.77 \times 10^{-3}$ over the range $z = [1.51, 4.4]$, we see excellent agreement. This agreement in Ω_g between the radio and optically-selected surveys for DLAs is the best evidence for our conclusion that dust bias does not have a major effect on the results of optically-selected surveys.

A.M.W., R.A.J., & J.X.P. are partially supported by the National Science Foundation grant AST-0307824.

E.G. acknowledges support from the National Science Foundation under grant AST-0201667, an NSF Astronomy and Astrophysics Postdoctoral Fellowship (AAPF).

REFERENCES

- Bennett, C.L., et al. 2003, *ApJS*, 148, 1
 Ellison, S.L., Yan, L., Hook, I.M., Pettini, M., Wall, J.V., & Shaver, P. 2001, *A&A*, 379, 393
 Fall, S.M. & Pei, Y.C. 1993, *ApJ*, 402, 479
 Gehrels, N. 1986, *ApJ*, 303, 336
 Henstock, D.R., Browne, I.W.A., Wilkinson, P.N., Taylor, G.B., Vermeulen, R.C., Pearson, T.J., Readhead, A.C.S. 1995, *ApJS*, 100, 1
 Henstock, D.R., Browne, I.W.A., Wilkinson, P.N., McMahon, R.G. 1997, *MNRAS*, 290, 380
 Jackson, C.A., Wall, J.V., Shaver, P.A., Kellerman, K.I., Hook, I.M., & Hawkins, M.R.S. 2002, *A&A*, 386, 97
 Kuhlbrodt, B., Orndahl, E., Wisotzki, L., & Jahnke, K. 2005, *A&A*, 439, 497
 Lanzetta, K. M., Wolfe, A. M., Turnshek, D. A., Lu, L., McMahon, R. G., & Hazard, C. 1991, *ApJS*, 77, 1
 Lu, L., Wolfe, A. M., Turnshek, D. A., & Lanzetta, K. M. 1993, *ApJ*, 84, 1
 Murphy, M.T., & Liske, J. 2004, *MNRAS*, 354, L31
 Murphy, et al. 2005, private communication
 Oke, J. B., Cohen, J. G., Carr, M., Cromer, J., Dingizian, A., Harris, F. H., Labrecque, S., Lucinio, R., Schaal, W., Epps, H., Miller, J. 1995, *PASP*, 107, 375
 Pearson, T. J. & Readhead, A. C. S. 1988, *ApJ*, 328, 114
 Péroux, C., Storrie-Lombardi, L.J., McMahon, R.G., Irwin, M., & Hook, I.M. 2001, *AJ*, 121, 1799
 Péroux, C., McMahon, R., Storrie-Lombardi, L., & Irwin, M.J. 2003, *MNRAS*, 346, 1103
 Pei, Y.C., & Fall, S.M. 1995, *ApJ*, 454, 69
 Pettini, M., Ellison, S.L., Steidel, C.C., Bowen, D.V. 1999, *ApJ*, 510, 576
 Polatidis A.G., Wilkinson P.N., Xu W., Readhead A.C.S., Pearson T.J., Taylor G.B., & Vermeulen R.C. 1995, *ApJS*, 98, 1
 Prochaska, J.X., Herbert-Fort, S., & Wolfe, A. M. 2005, Accepted to *ApJ*, astro-ph/0508361 (PHW05)
 Prochaska, J.X. 2003, *IAU*,
 Rao, S.M. & Turnshek, D.A. 2000, *ApJS*, 130, 1
 Sargent, W. L. W., Steidel, C. C., & Boksenberg, A. 1989, *ApJS*, 69, 703
 Sheinis, A. I., Bolte, M., Epps, H. W., Kibrick, R. I., Miller, J. S., Radovan, M. V., Bigelow, B. C., Sutin, B. M. 2002, *PASP*, 114, 851
 Taylor, G.B., et al. 1994, *ApJS*, 95, 345
 Taylor, G. B., Vermeulen, R. C., Readhead, A. C. S., Pearson, T. J., Henstock, D. R., Wilkinson, P. N. 1996, *ApJS*, 107, 37
 Thakkar D.D., Xu W., Readhead A.C.S., Pearson T.J., Taylor G.B., Vermeulen R.C., Polatidis A.G., Wilkinson P.N. 1995, *ApJS*, 98, 33
 Veron-Cetty, M.-P. & Veron, P. 1993, *ESO Scientific Report No. 13*
 Wild, V. & Hewett, P. 2005, *MNRAS*, 361, L30
 Wolfe, A. M., Lanzetta, K. M., Foltz, C. B., and Chaffee, F. H. 1995, *ApJ*, 454, 698
 Wolfe, A. M., Prochaska, J.X., & Gawiser, E. 2003, *ApJ*, 593, 215
 Wolfe, A. M., Gawiser, E., & Prochaska, J.X. 2005, *ARA&A*, 43, 861

Wright, A. & Ostrupcek, R. 1990, Parkes Catalog, Australia
Telescope National Facility
Xu W., Readhead A.C.S., Pearson T.J., Polatidis A.G., Wilkinson
P.N. 1995, ApJS, 99, 297